

Gravitational lensing of cosmic microwave background anisotropies and cosmological parameter estimation

R. Stompor^{*} and G. Efstathiou

Institute of Astronomy, Madingley Road, Cambridge CB3 0HA
E-mail: radek@ast.cam.ac.uk; gpe@ast.cam.ac.uk

26 December 2017

ABSTRACT

Gravitational lensing, caused by matter perturbations along the line-of-sight to the last scattering surface, can modify the shape of the cosmic microwave background (CMB) anisotropy power spectrum. We discuss the detectability of lensing distortions to the temperature, polarisation and temperature-polarisation cross-correlation power spectra and we analyse how lensing might affect the estimation of cosmological parameters. For cold dark matter-like models with present-day matter power spectra normalised to match the abundances of rich clusters of galaxies, gravitational lensing causes detectable distortions to cosmic variance limited CMB experiments sampling high multipoles ($\ell \gtrsim 1000$). Gravitational lensing of the CMB, although a small effect, allows independent determinations of the curvature of the universe and the cosmological constant, i.e. breaking the so-called *geometrical degeneracy* in CMB parameter estimation discussed by Bond, Efstathiou & Tegmark (1997) and Zaldarriaga, Spergel & Seljak (1997). Gravitational lensing of the CMB temperature and polarisation patterns should be detectable by the Planck Surveyor satellite leading to useful independent constraints on the cosmological constant and spatial curvature.

Key words: cosmic microwave background anisotropies – gravitational lensing, cosmological parameters estimation

1 INTRODUCTION AND MOTIVATION

Since the early papers on the cosmic microwave background anisotropies (CMB) by Peebles & Yu (1968), Doroshkevich, Zel'dovich, & Sunyaev (1978), Wilson & Silk (1981) and others, it has been evident that the CMB anisotropies are sensitive to fundamental cosmological parameters. These include parameters that define the background cosmology (such as the geometry and matter content) and parameters that define the nature of irregularities in the early Universe (such as the amplitude and shape of the fluctuation spectrum). Early attempts to constrain the parameters of cold dark matter (CDM) models were made by Bond & Efstathiou (1984) and Vittorio & Silk (1984). More recently, the parameters of CDM-type models have been constrained using the *COBE*–DMR data alone (e.g. Bennett et al. 1996, Bunn, Scott & White 1995, Stompor, Górski & Banday 1995, Górski et al. 1998), and *COBE* combined with degree-scale measurements of CMB anisotropies (e.g. Hancock et al. 1997, Lineweaver et al. 1997, Bond & Jaffe 1997).

In the near future, long-duration balloon flights and

satellite experiments promise to provide a wealth of high quality data on the CMB anisotropies. This has stimulated a number of theoretical investigations on the determination of cosmological parameters from observations of the CMB anisotropies (e.g. Jungman et al. 1996, Bersanelli et al. 1996, Bond, et al. 1997, Zaldarriaga et al. 1997, Efstathiou & Bond 1998, Eisenstein, Hu & Tegmark 1998). These studies have confirmed that many cosmological parameters, or combinations of parameters, can be determined by future satellite missions to unprecedented precisions of a few percent or better. However, these studies have identified some degeneracies between sets of cosmological parameters[†] estimated from the linear CMB power spectra alone. Since the entire statistical information on the CMB anisotropies in Gaussian theories is contained in the power spectrum, such parameter degeneracies impose serious limitations on the ability of CMB experiments to constrain cosmological parameters without invoking additional external constraints.

In particular, Bond et al. (1997) and Zaldarriaga et al. (1997) have emphasized that cosmological models with

^{*} on the leave of absence from Copernicus Astronomical Centre, Warszawa, Poland

[†] i.e. parameter sets that lead to almost indistinguishable CMB power spectra.

identical fluctuation spectra, matter content and angular diameter distance to the scattering surface (see Section 2.1 below) will produce statistically almost indistinguishable power spectra of CMB fluctuations. This property (which we call the *geometrical degeneracy* hereafter) means that in the limit of validity of linear perturbation theory, CMB measurements cannot set strong independent bounds on the spatial curvature and cosmological constant and hence cannot unambiguously constrain the spatial geometry of the Universe.

In fact there are many additional observational constraints that can be used to break the geometrical degeneracy. Examples include accurate measurements of the Hubble constant, the age of the Universe and the geometrical constraints imposed by Type Ia supernovae light curves [see Figure 1 and the more detailed discussions by White (1998), Tegmark, Eisenstein & Hu (1998) and Efstathiou & Bond (1998)]. However, before invoking more conventional astronomical observations, it is worthwhile analysing whether there are non-linear contributions to the CMB anisotropies that can break the geometrical degeneracy. If such effects are present, then it may be possible to break the geometrical degeneracy using measurements of the CMB alone. In this paper, we analyse the effect of gravitational lensing on the CMB anisotropies. Although acknowledged to be small (Blanchard & Schneider 1987, Cole & Efstathiou 1989, Sasaki 1989, Seljak 1996), the gravitational lensing effect may be detectable by the high precision observations of the CMB anisotropies expected from future satellite experiments. The possibility of utilising gravitational lensing to break the geometrical degeneracy has been noticed independently by Metcalf & Silk (1998). In this paper, we analyse the effects of gravitational lensing on the temperature, polarisation and temperature-polarisation cross-correlation power spectra and assess whether it is possible to observe these effects with the MAP (Bennett et al. 1997) and Planck (Bersanelli et al. 1996) satellites.

2 THE GEOMETRICAL DEGENERACY

2.1 Physical mechanism

In this paper we restrict ourselves to cold dark matter (CDM) cosmologies with adiabatic scalar perturbations, an arbitrary value of the curvature ($\Omega_K \equiv -K/H_0^2$) and cosmological constant ($\Omega_\Lambda \equiv \Lambda/3H_0^2$). Following Bond et al. (1997) we use physical densities, $\omega_i \equiv \Omega_i h^2$, to define the matter content of the universe \ddagger , with $i = K, \Lambda, b, c, \gamma, \dots$, and $\Omega_b, \Omega_c, \Omega_\gamma, \dots$ are the density parameters of baryons, cold dark matter (CDM), photons etc. We assume the standard thermal history throughout this paper with recombination at redshift $z \sim 1100$ (Peebles 1968) and ignore the possibility of reionization. In the numerical examples described below, we have assumed a scale-invariant (Harrison-Zel'dovich) power spectrum of primordial scalar and adiabatic fluctuations i.e. $\propto \sqrt{k^2 + K}$, where a wavenumber k is the separation constant of the Helmholtz equation (e.g. Harrison 1967).

\ddagger Where h is the Hubble's constant H_0 in units of $100 \text{ kms}^{-1} \text{ Mpc}^{-1}$.

As is well known, the power spectrum of the CMB anisotropies in such models displays prominent ‘Doppler’ peaks (see, e.g. Figures 2a,b). The shape of the CMB power spectrum and, in particular, the locations and relative heights of the peaks, depend sensitively on cosmological parameters (e.g. Hu & Sugiyama 1995). The Doppler peak structure is imprinted into the present day CMB power spectrum at the time of recombination. Since recombination occurs at a high redshift, no plausible value of the cosmological constant or spatial curvature can influence the dynamical evolution of the universe at that time \S . The statistical properties of the CMB anisotropies at the time of last scattering are therefore determined by the form of the initial fluctuations spectrum (mode, shape and amplitude) and by the physical densities that determine the sound speed prior to recombination.

After last scattering, (assuming that the universe remains neutral) the only mechanism that can affect a freely-falling CMB photon is the gravitational interaction with the evolving matter field. In the linear approximation this is sometimes called the integrated Sachs-Wolfe effect [see, e.g. the review by Bond (1996)] and is of importance only for temperature fluctuations on the largest angular scales. Since the large-scale anisotropies have large statistical uncertainties (cosmic variance), the integrated Sachs-Wolfe effect cannot break the geometrical degeneracy except for extreme values of the cosmological parameters [see Efstathiou & Bond (1998) for detailed calculations]. In linear theory, the geometrical degeneracy can be assumed to be exact for most practical purposes.

Two models will have statistically indistinguishable temperature, polarisation and cross-correlation linear power spectra as a result of the geometrical degeneracy if they have:

- (i) identical matter content of those components that determine the sound speed at recombination, $\omega_c, \omega_b, \dots$;
- (ii) identical comoving distance to the last scattering surface (r_{LS}), where

$$\frac{r_{LS}}{3000 \text{ Mpc}} = \frac{1}{\sqrt{\omega_K}} \sinh \left[\int_{a_{LS}}^{a_0} \frac{\omega_K^{1/2} da}{\sqrt{\omega_K a^2 + \omega_\Lambda a^4 + \omega_m a}} \right], \quad (1)$$

$\omega_m \equiv \omega_c + \omega_b$, (Bond et al. 1997). In equation (1) we have assumed an open universe ($\omega_K > 0$). The upper limit in (1) is the value of the scale factor a at the present epoch and the lower limit is the value at the time of the last scattering [for which we use the fitting formula of Hu & White (1997)];

- (iii) identical fluctuation spectra normalised to have the same amplitudes at the time of recombination.

If the above conditions are satisfied, the CMB power spectra of the two models will be indistinguishable on small angular scales, but will differ at large angles because of geometrical effects on near curvature scales and, in the case of temperature anisotropies, through the integrated Sachs-Wolfe effect. However, these effects are weak discriminators of models.

\S We do not consider the possibility of a dynamically evolving cosmological constant or ‘quintessence’-like component as discussed by Ratra & Peebles (1988), Turner & White (1997), Caldwell, Dave & Steinhardt (1998), Huey et al. (1998)

In the analysis that follows, when we compare two models, we normalise them so that the root mean square mass deviation computed within a top hat window of radius $R = 8h^{-1}\text{Mpc}$ [denoted hereafter $\sigma_R(t)$] is the same *at the time of last scattering* ($t = t_{LS}$). This prescription determines the relative normalisations of any two models that we wish to compare, but does not determine the absolute normalisation.

The effects of gravitational lensing depend, of course, on the absolute normalisation of the matter fluctuations. We therefore normalise a given target model so that the rms mass fluctuations within a sphere of $8h^{-1}\text{Mpc}$ at the present day ($t = t_0$) reproduces the abundances of rich clusters of galaxies. We therefore impose the constraint,

$$\sigma_8(t_0) = (0.52 \pm 0.12) \Omega_m^{-0.47}, \quad (2)$$

from the recent analysis of Eke, Cole & Frenk (1996). The normalisation of scale-invariant models derived from (2) is usually lower than that inferred from the 4 year COBE-DMR data (e.g. Górski et al. 1998). However, equation (2) provides a more direct measure of the amplitude of the mass fluctuations which generate gravitational lensing effects at recent epochs.

We give the 1σ uncertainty in equation (2), though this is sufficiently small that it has no significant effect on results described below. Some authors, e.g. Viana & Liddle (1996) deduce slightly larger values of $\sigma_8(t_0)$ for low density models, in which case our analysis will underestimate the effects of gravitational lensing on the CMB.

In summary, we pick a specific set of cosmological parameters to define a target model and we use equation (2) to set the absolute normalisation of the fluctuation spectrum. When we compare models with a different set of cosmological parameters, we choose a normalisation so that the fluctuation spectra have the same amplitude at the time of recombination, so preserving the geometrical degeneracy.

These points are illustrated in Figures 1 and 2. Figure 1 shows degenerate loci in the ω_K , ω_Λ plane ($r_{LS} = \text{constant}$) for models with $\omega_m = 0.1$ and $\omega_b = 0.0125$. Figures 2a,b show the linear CMB power spectra for two sets of models satisfying the geometrical degeneracy plotted as filled circles in Figure 1. These have been computed using a version of the CMBFAST code developed by Seljak & Zaldarriaga (1996) which we have modified to gain an improvement in accuracy (see Section 4.2). Clearly, the spectra for each set of models are almost indistinguishable. The only significant deviations are at low multipoles ($\ell \lesssim 100$) and are a consequence of the integrated Sachs-Wolfe effect described above. In fact, the numerically computed spectra in Figures 2a,b also show some residual differences at high ℓ (illustrated by the dashed line in the middle panels of Figure 2a,b). However, these differences are dominated by residual numerical inaccuracies in CMBFAST (see the discussion in Section 4.2). For models with reasonable normalisations [i.e. reproducing cluster abundances as inferred from equation (2)] these numerical errors are much smaller than differences arising from gravitational lensing.

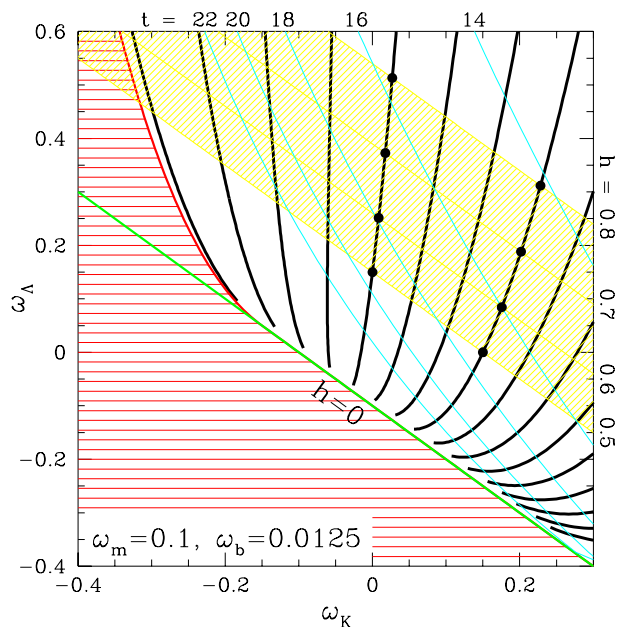


Figure 1. The $\omega_K - \omega_\Lambda$ plane showing the sets of models (curved thick solid lines) satisfying the geometrical degeneracy and hence having nearly indistinguishable power spectra according to linear perturbation theory. These curves are computed for the models with $\omega_m = 0.1$, and $\omega_b = 0.0125$. Lines of constant Hubble parameter values (solid thin straight lines labelled with Hubble parameter values at the right edge of the figure), and of constant age (solid thin lines labelled at the top of the figure with the age in Gyr) are also shown. Filled circles show the two families of nearly degenerate models with power spectra plotted in Figures 2a,b. The parameters of these models are listed in Table 1.

2.2 Degeneracy lines

If we keep all of the parameters of a target model fixed but vary ω_K and ω_Λ , the geometrical degeneracy will be satisfied if

$$\delta\omega_K \left(\frac{\partial r_{LS}}{\partial \omega_K} \right)_0 + \delta\omega_\Lambda \left(\frac{\partial r_{LS}}{\partial \omega_\Lambda} \right)_0 \simeq 0, \quad (3)$$

where the subscript 0 on any quantity denotes that it is computed assuming the parameters of the target model. We can define two new parameters ω_\parallel and ω_\perp ,

$$\begin{bmatrix} \omega_\parallel \\ \omega_\perp \end{bmatrix} \equiv \begin{bmatrix} \cos \phi & \sin \phi \\ -\sin \phi & \cos \phi \end{bmatrix} \begin{bmatrix} \delta\omega_K \\ \delta\omega_\Lambda \end{bmatrix}, \quad (4)$$

where $\phi \equiv -\arctan \left[\left(\frac{\partial r_{LS}}{\partial \omega_\Lambda} \right)_0^{-1} \left(\frac{\partial r_{LS}}{\partial \omega_K} \right)_0 \right]$ is the angle between a degenerate curve plotted in Figure 1 and the ω_K axis. Models satisfying $\omega_\perp = 0$ thus have the same value of r_{LS} for small variations of parameters and therefore satisfy the geometrical degeneracy. Hereafter we call any direction with $\omega_\perp = 0$ a degeneracy direction. If the geometrical degeneracy were perfect, the derivative of the CMB power spectrum along a degeneracy direction should be exactly equal to zero. The numerical derivatives of linear power spectra are discussed in section 4.2 (see also Efstathiou & Bond 1998) and shown in Figures 4 & 8.

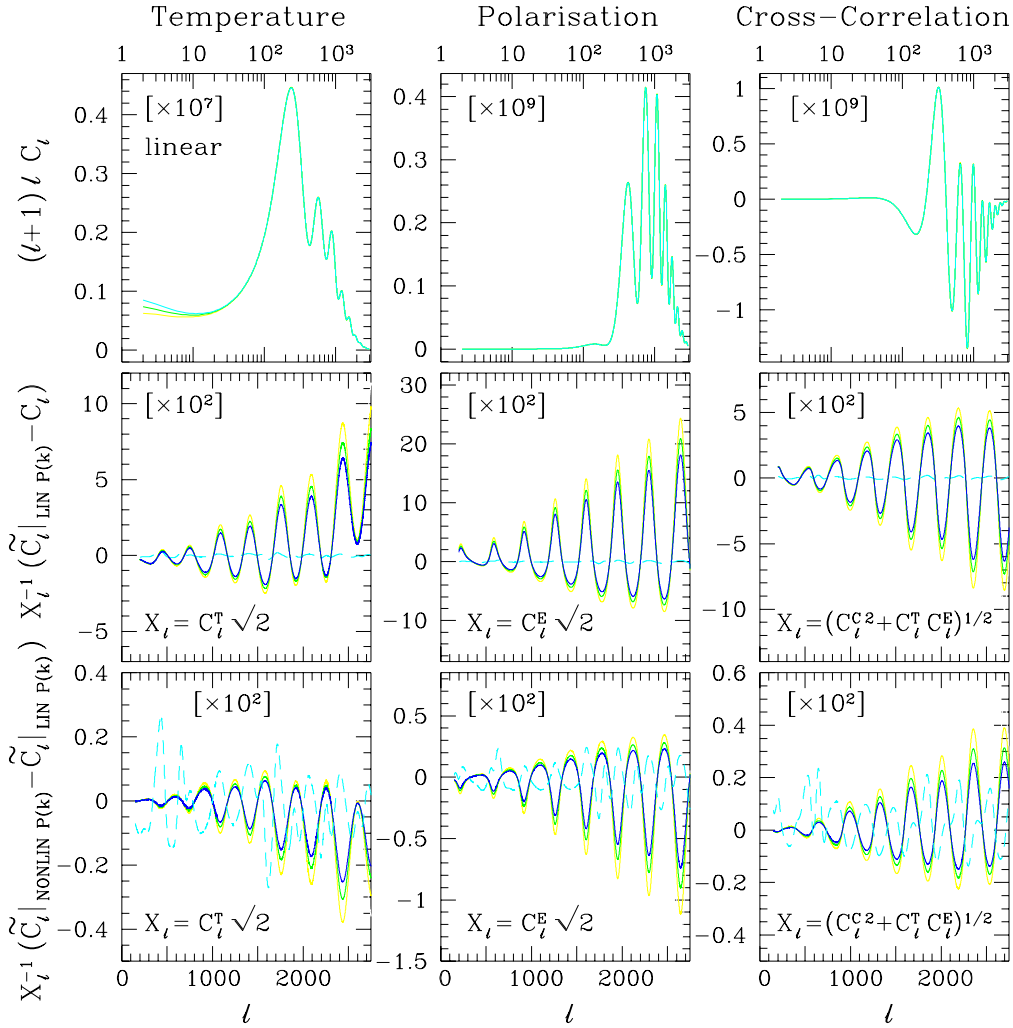


Figure 2. (a) The four lines in each panel of the **top row** show nearly identical linear temperature, polarisation and cross-correlation power spectra for each of four nearly degenerate models (models of class 1 listed in Table 1). **Middle row:** The solid lines show the gravitational lensing contribution assuming only the linear matter power spectrum at all epochs. The solid lines in the **bottom panels** show the changes of gravitational lensing contribution caused by the non-linear corrections to the matter power spectrum evolution (implemented through the Peacock & Dodds (1996) formalism). The dashed lines in the middle and lower row show the typical differences between linear radiation power spectra plotted in the top row. Note that the X_ℓ quantity used to normalise the gravitational lensing contributions in the two bottom rows is proportional to the cosmic variance (e.g. eqn. 14). The normalisation for target model (model 1a) is fixed according to the present-day cluster abundances (eqn. 2). The remaining models are required to have, the same amplitude of the fluctuations at the time of last scattering. The presented results have been multiplied by factors as given in each panel.

3 GRAVITATIONAL LENSING CONTRIBUTION

3.1 Formalism

The gravitational lensing contribution to the temperature power spectra has been computed in the past by several authors (e.g. Blanchard & Schneider 1987, Cole & Efstathiou 1989, Sasaki 1989, Seljak 1996, Martínez-González, Sanz & Cayón 1997, Zaldarriaga & Seljak 1998). Here we follow the approach of Seljak (1996) and Zaldarriaga & Seljak (1998). We denote the linear power spectra as C_ℓ^T , C_ℓ^E and C_ℓ^C for temperature, polarisation (E-component only) and their cross-correlation respectively. The CMB spectra including the gravitational lensing contribution are assigned a tilde.

The full radiation power spectra including gravitational

lensing can be expressed as convolutions of the corresponding linear spectra ($I = T, E, C$),

$$\tilde{C}_\ell^I = C_\ell^I + \sum_{\ell'} \mathcal{W}_{\ell\ell'}^I C_{\ell'}^I \quad (5)$$

where the window functions $\mathcal{W}_{\ell\ell'}^I$ are given as,

$$\mathcal{W}_{\ell\ell'}^T = \frac{\ell'^3}{2} \int_0^\infty d\theta \theta [\sigma_2^2(\theta) J_2(\ell'\theta) - \sigma^2(\theta) J_0(\ell'\theta)] J_0(\ell\theta) \quad (6)$$

$$\mathcal{W}_{\ell\ell'}^E = \frac{\ell'^3}{4} \int_0^\infty d\theta \theta \left\{ \frac{\sigma_2^2}{2}(\theta) [J_2(\ell'\theta) + J_6(\ell'\theta)] - \sigma^2(\theta) J_4(\ell'\theta) \right\} J_4(\ell\theta) + \frac{1}{2} \mathcal{W}_{\ell\ell'}^T \quad (7)$$

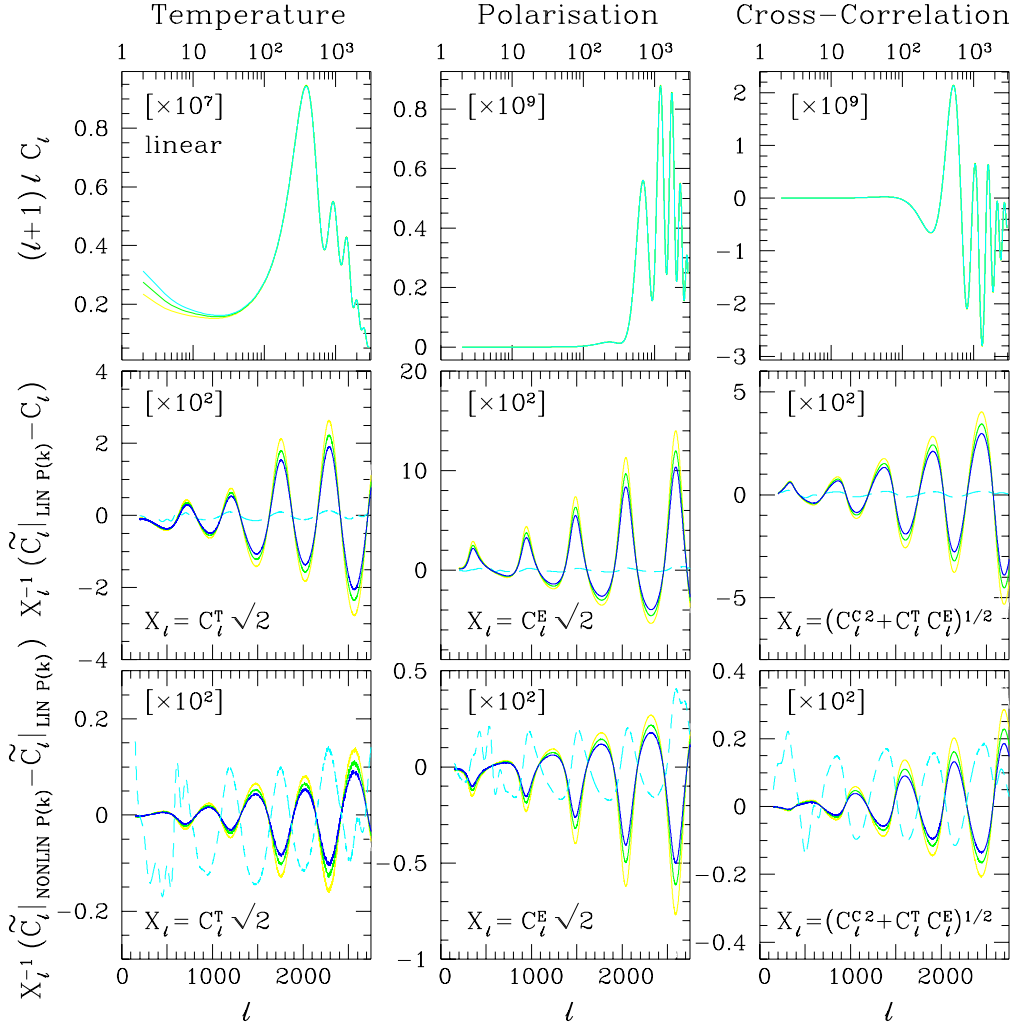


Figure 2. (b) As figure 2a but for the second class of models with parameters listed in Table 1.

$$\mathcal{W}_{\ell\ell'}^C = \frac{\ell^3}{2} \int_0^\infty d\theta \theta \left\{ \frac{\sigma_2^2}{2}(\theta) [J_0(\ell'\theta) + J_4(\ell'\theta)] - \sigma^2(\theta) J_2(\ell'\theta) \right\} J_2(\ell\theta) \quad (8)$$

and photon path dispersions,

$$\sigma^2(\theta) = 16\pi^2 \int_0^\infty dk k^3 \int_0^{\chi_{LS}} d\chi P_\phi(k, \tau_0 - \chi) \times W^2(\chi, \chi_{LS}) [1 - J_0(k\theta \sin_K \chi)]; \quad (9)$$

$$\sigma_2^2(\theta) = 16\pi^2 \int_0^\infty dk k^3 \int_0^{\chi_{LS}} d\chi P_\phi(k, \tau_0 - \chi) \times W^2(\chi, \chi_{LS}) J_2(k\theta \sin_K \chi). \quad (10)$$

Here τ denotes a conformal time, $\chi \equiv \tau_0 - \tau$ (subscripts 0 and LS denote values at the present and last scattering respectively), and $P_\phi(k, \tau)$ is the power spectrum of the gravitational potential of the matter perturbations. The window function $W(\chi, \chi_{LS})$ is given by the expression:

$$W^2(\chi, \chi_{LS}) = \frac{\sin_K(\chi_{LS} - \chi)}{\sin_K \chi_{LS}}, \quad (11)$$

where $\sin_K \chi$ gives the distance traveled by the photon emitted at $\tau_0 - \chi$ i.e.

$$\sin_K \chi = \begin{cases} K^{-1/2} \sin K^{1/2} \chi, & K > 0; \\ \chi, & K = 0; \\ (-K)^{1/2} \sinh(-K)^{1/2} \chi, & K < 0. \end{cases} \quad (12)$$

The above set of equations has been derived recently by Zaldarriaga & Seljak (1998) [see Zaldarriaga & Seljak (1998) equations (7)-(10)], except that we have set the upper limit of the θ -integration in equations (6-8) to infinity to ensure the correct asymptotic limit $\tilde{C}_\ell \rightarrow C_\ell$ for $\sigma(\theta), \sigma_2(\theta) \rightarrow 0$.

The gravitational lensing correction to the CMB anisotropies depends on the full matter power spectrum, including non-linear contributions from small spatial scales. Previous calculations (e.g. Cole & Efstathiou 1989, Seljak 1996, Zaldarriaga & Seljak 1998) have suggested that the contribution of non-linear modes introduces only minor corrections to the gravitational lensing contribution computed using the linear form of the matter power spectrum. To check whether non-linear evolution affects our analysis we have modelled the non-linear corrections to the matter power spectrum using the approach of Peacock & Dodds (Peacock

Table 1. Parameters of the cosmological models discussed in this paper.

	ω_m	ω_b	ω_K	ω_Λ	h	$\sigma_8(t_0)$
• standard CDM model:	0.25	0.125	0.0	0.0	0.5	0.52
• class 1 of models:						
(a)	0.1	0.0125	0.0	0.15	0.5	0.8
(b)	0.1	0.0125	0.0085	0.2515	0.6	0.95
(c)	0.1	0.0125	0.0174	0.3726	0.7	1.1
(d)	0.1	0.0125	0.0269	0.5131	0.8	1.24
• class 2 of models:						
(a)	0.1	0.0125	0.15	0.0	0.5	0.8
(b)	0.1	0.0125	0.1756	0.0844	0.6	0.95
(c)	0.1	0.0125	0.2018	0.1882	0.7	1.1
(d)	0.1	0.0125	0.2284	0.3116	0.8	1.24

& Dodds 1996). For values of $\sigma_8(t_0)$ given in equation (2), the Peacock-Dodds non-linear corrections are indeed small contributions (see the bottom panels of Figures 2a,b) and can be neglected for most purposes.

Recently Zaldarriaga and Seljak (1998) released a version of CMBFAST that includes gravitational lensing. A comparison between our code and theirs shows good agreement with differences smaller than 5% of a lensing generated contribution.

3.2 Detectability

To assess whether the lensing effects are detectable, we analyse the two classes of degenerate models illustrated in Figures 1 and 2. Models of the first class (hereafter Class 1) have power spectra which are indistinguishable from that of a spatially flat cosmological model with $\omega_m = 0.1$, $\omega_b = 0.0125$ and $\omega_\Lambda = 0.15$. Class 2 models have power spectra that are indistinguishable with that of an open universe with zero cosmological constant, $\omega_m = 0.1$, $\omega_b = 0.0125$ and $\omega_K = 0.15$. The models in each class are labelled with a letter, (a, b, c, d) in ascending order of the value of the Hubble constant ($h = 0.5, 0.6, 0.7, 0.8$). For all models we assume a precisely scale-invariant spectrum of scalar adiabatic perturbations and no contribution from tensor modes.

The parameters for the two families of models are specified in Table 1. For comparison we have also computed results for the ‘standard’ CDM model [$\omega_m = 0.25$, $\omega_b = 0.0125$, $\omega_K = \omega_\Lambda = 0$, $\sigma_8(t_0) = 0.52$; hereafter SCDM]. To explore how the results depend on the spatial resolution of the CMB observations, we have analysed idealized examples of cosmic variance limited observations of the power spectrum with upper multipole limits of $\ell_{\max} = 1000, 2000$ and 2750. Also, to assess how more realistic observations might perform, we investigate two experimental set-ups corresponding approximately to the MAP and Planck satellite missions. The assumed specifications are as follows: (1) the improved MAP (¶) best channel parameters (hereafter MAP+) with a total power detector noise $w_T^{-1} = 2.3 \times 10^{-15}$

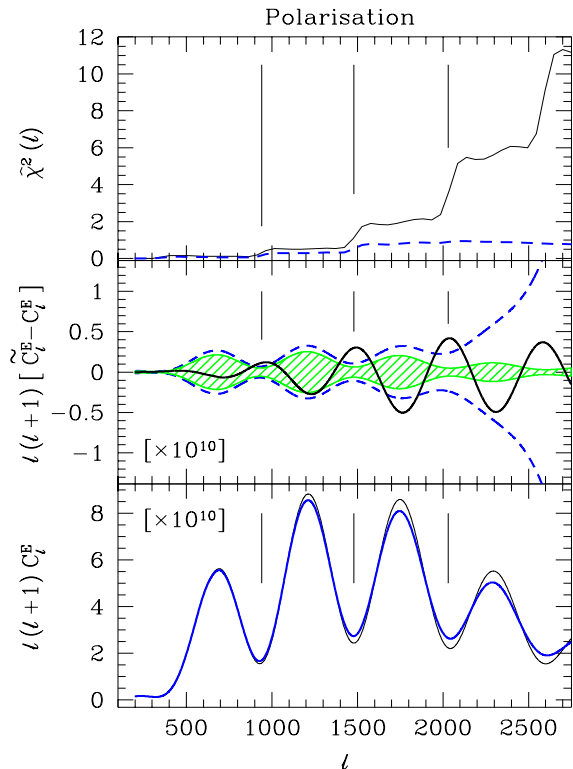


Figure 3. The top panel shows the dependence of the reduced χ^2 (equation 13) on the value of the high- ℓ cutoff for a cosmic variance limited (solid line) and a Planck-type observation (dashed line) of the polarisation power spectrum. The thick oscillatory line in the middle panel shows the gravitational lensing correction compared with the statistical uncertainties of a cosmic variance limited experiment (shaded region) and a Planck-like experiment (region delimited by dashed lines). The corresponding linear (thick solid line) and total lensed power spectra (thin solid line) are shown in the bottom panel. The results shown in these figures are for model 2a with parameters listed in Table 1. The vertical thin lines in each panel show the positions of minima in the linear power spectrum. The jumps in the reduced χ^2 (top panel) occur at the minima because that is where the lensing correction is the largest and the cosmic variance is the smallest.

and a resolution $\theta_{fwhm} = 13.5'$; (2) the 90GHz, 150GHz and 220GHz of the Planck (¶) satellite: $w_{T(1)}^{-1} = 2.8 \times 10^{-17}$, $\theta_{fwhm(1)} = 16'$; $w_{T(2)}^{-1} = 1.5 \times 10^{-17}$, $\theta_{fwhm(2)} = 10'$; and $w_{T(3)}^{-1} = 0.5 \times 10^{-17}$, $\theta_{fwhm(3)} = 6.6'$. The numbers and notation follow those of Bond et al. (1997) with w_T^{-1} defined for a single channel as the squared product of the noise level per pixel and the angular size of a pixel. The polarisation detector noise is assumed to be 1.5 and 2 times that of the total power noise for MAP and Planck (see Puget et al. 1998 for a recent discussion of the polarisation characteristics of the Planck HFI) respectively. In analysing both satellites, we assume that Galactic emission is negligible (or subtractable to high accuracy) over a fraction $f_{sky} = 0.65$ of the sky.

We assess the amplitude of the gravitational lensing corrections to C_ℓ by computing the reduced χ^2 ,

¶ see the MAP homepage: <http://map.gsfc.nasa.gov>.

¶ see the Planck homepage: <http://astro.estec.esa.nl/SA-general/Projects/Planck>.

Table 2. $\hat{\chi}^2$ statistics (see eqn. 13) computed for the two classes of models defined in Table 1 and for the experimental parameters defined in Section 3.2. The effective beam cutoffs (ℓ_{beam}) for the satellite missions are given in the second row. ℓ_{max} denotes the number of C_ℓ coefficients included in the sum of equation (13). The value of ℓ_{max} is equal to the cut-off in ℓ -space for cosmic variance limited experiments and it is chosen to maximize $\hat{\chi}^2$ (see figure 3) for Map and Planck. The results are given for temperature (T), polarisation (E) and cross-correlation (C) power spectra.

	cosmic variance limited experiment									MAP+			PLANCK		
	$\ell_{\text{max}} = 1000$			$\ell_{\text{max}} = 2000$			$\ell_{\text{max}} = 2750$			$\ell_{\text{beam}} \sim 600$			$\ell_{\text{beam}} \sim 1220$		
	T	E	C	T	E	C	T	E	C	T	E	C	T	E	C
• standard CDM model: $\omega_m = 0.25, \omega_b = 0.125$										$\ell_{\text{max}} \simeq 400$	400	500	2200	1350	1600
	0.02	0.15	0.08	0.2	2.2	0.8	7.3	9.2	3.4	$\lesssim 10^{-2}$	$\lesssim 10^{-2}$	$\lesssim 10^{-2}$	0.09	0.07	0.1
• class 1 of models: $\omega_m = 0.1, \omega_b = 0.0125$										$\ell_{\text{max}} \simeq 1000$	600	900	2500	1800	1950
(1a)	0.07	0.9	0.3	0.9	12.5	4.2	4.8	33.0	12.2	0.02	$\lesssim 10^{-3}$	$\lesssim 10^{-2}$	0.8	1.5	1.2
(1b)	0.09	1.2	0.4	1.1	16.3	5.5	6.11	42.8	15.8	0.02	$\lesssim 10^{-3}$	$\lesssim 10^{-2}$	1.2	2.2	1.7
(1c)	0.1	1.6	0.55	1.5	21.2	7.1	7.8	55.6	20.4	0.03	$\sim 10^{-3}$	$\sim 10^{-2}$	1.7	3.4	2.5
(1d)	0.13	2.0	0.7	1.8	26.2	8.7	9.5	68.3	25.1	0.05	$\sim 10^{-3}$	$\sim 10^{-2}$	2.3	4.7	3.2
• class 2 of models: $\omega_m = 0.1, \omega_b = 0.0125$										$\ell_{\text{max}} \simeq 1000$	760	850	2650	2100	2500
(2a)	0.02	0.5	0.07	0.3	2.6	1.3	0.8	11.2	4.7	0.01	$\lesssim 10^{-2}$	$\sim 10^{-2}$	0.4	0.95	0.75
(2b)	0.02	0.7	0.08	0.35	3.45	1.7	1.0	14.5	6.2	0.01	$\lesssim 10^{-2}$	$\lesssim 10^{-2}$	0.6	1.5	1.1
(2c)	0.03	0.9	0.1	0.45	4.5	2.2	1.3	18.6	7.9	0.01	$\lesssim 10^{-2}$	$\lesssim 10^{-2}$	0.75	2.2	1.6
(2d)	0.03	1.1	0.13	0.55	5.5	2.7	1.6	22.7	9.7	0.02	$\lesssim 10^{-2}$	$\lesssim 10^{-2}$	0.9	3.0	2.1

$$\hat{\chi}^2 = \frac{1}{\ell_{\text{max}}} \sum_{\ell=2}^{\ell_{\text{max}}} \frac{(\tilde{C}_\ell - C_\ell)^2}{(\Delta C_\ell)^2}, \quad (13)$$

where \tilde{C}_ℓ is the gravitationally lensed power spectrum computed from equation (5), C_ℓ is the unlensed linear power spectrum, and ΔC_ℓ is the variance of C_ℓ given as,

$$\begin{aligned} [\Delta C_\ell^{T,E}]^2 &\equiv \frac{2}{(2\ell+1)f_{sky}} (C_\ell^{T,E} + w_{T,E}^{-1} b_\ell^{-2})^2, \\ [\Delta C_\ell^C]^2 &\equiv \frac{1}{(2\ell+1)f_{sky}} \left[(C_\ell^C)^2 + \right. \\ &\quad \left. + (C_\ell^T + w_T^{-1} b_\ell^{-2}) (C_\ell^E + w_E^{-1} b_\ell^{-2}) \right], \end{aligned} \quad (14)$$

for an observation with N antennae of different sensitivities and Gaussian beam widths $\sigma_{b(i)}$, $i = 1, \dots, N$. The total noise level $w_{T,E}$ in equation (10) is the sum of the respective noise levels for each of the channels ($w_{T,E(i)}$), and an effective beam shape b_ℓ is given by (Bond et al. 1997), $b_\ell = w_{T,E}^{-1} \sum_i w_{T,E(i)} \exp[-\ell(\ell+1)\sigma_{b(i)}^2]$. For cosmic variance limited experiments, ℓ_{max} in equation (13) is equal to the adopted cut off in an ℓ space. For the MAP and Planck satellite, we choose the value ℓ_{max} that maximizes $\hat{\chi}^2$ as given in Table 2 (see also figure 3).

A value of $\hat{\chi}^2$ of order unity signifies that the lensing distortion is detectable in principle by an experiment. In this Section we use this criterion as a rough measure of the detectability of gravitational lensing in the CMB. However, if we parameterize C_ℓ by N cosmological parameters, then values of $\hat{\chi}^2$ as low as $\sim N/\ell_{\text{max}}$ can lead to significant differences between estimated parameters. The effect of lensing on cosmological parameters is discussed in more detail in Section 4.3.

Values of $\hat{\chi}^2$ are listed in Table 2 for various experimental setups. For cosmic variance limited observations, the reduced $\hat{\chi}^2$ values are approximately proportional to the fourth power of the mass spectrum normalisation amplitude $\sigma_8(t_0)$.

For the normalisation required by the observed present day cluster abundance (equation 2), the gravitational lensing contributions to the CMB power spectra are small but not negligible at the sensitivities of a Planck-type experiment. Since the lensing corrections depend strongly on the amplitude of the mass fluctuations at the relatively high redshifts, the detectability of lensing is sensitive to the parameters of the target model. Thus, the reduced $\hat{\chi}^2$ values for the standard CDM model listed in Table 2 for a Planck-type experiment are much lower than those of the Λ -dominated and open models listed in the table, which have higher values of σ_8 and lower perturbation growth rates at the present. Gravitational lensing modifies the ‘damping tail’ of the temperature power spectrum at high multipoles (Metcalf & Silk 1998) and this effect makes a significant contribution to $\hat{\chi}^2$ in cosmic variance limited experiments probing $\ell_{\text{max}} \gtrsim 2000$. The detectability of lensing is thus sensitive to the multipole range probed by an experiment and to the cosmological angle-distance relation; the effect of lensing is less easy to detect in a negatively curved universe since the damping tail is pushed to higher multipoles and power spectrum peaks are broader than in a spatially flat universe. This is why the $\hat{\chi}^2$ values in Table 2 for the $\omega_K = 0.15$ model are lower than those of the $\omega_K = 0$ model at fixed ℓ_{max} .

The effects of gravitational lensing on the polarisation power spectrum are even more significant than for the temperature power spectrum, producing significant distortions at $\ell \sim 1000$. At first sight the high values of $\hat{\chi}^2$ for polarisation might seem surprising. They arise because the polarisation power spectrum has sharper minima and peaks compared to the temperature power spectrum (cf. Figures 2a,b) and is therefore more sensitive to the gravitational lensing convolution (equation 5). This build up of $\hat{\chi}^2$ with multipole for polarisation is illustrated in Figure 3.

However, as the amplitude of the polarisation power spectrum is almost two orders of magnitude lower than that of the temperature fluctuations, an experiment with high

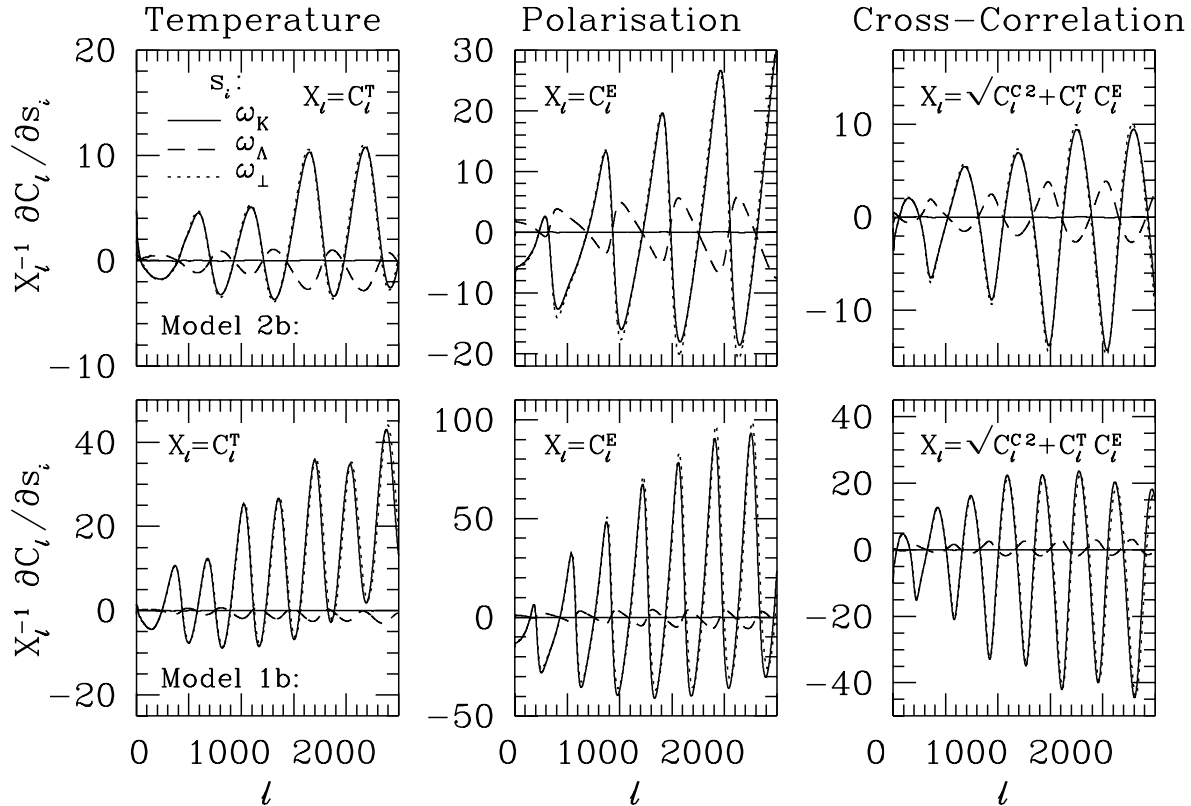


Figure 4. The derivatives of the linear power spectrum of temperature (left panels), polarisation (middle panels) and cross-correlation (right panels) with respect to ω_K (solid lines), ω_Λ (dashed), and ω_\perp (dotted). Model 2b is shown in the upper figures and model 1b in the lower figures. The nearly horizontal lines in each panel show the numerically computed derivative along the degeneracy direction [i.e. with respect to ω_\parallel see eqn.(4)].

sensitivity to polarisation, in addition to high angular resolution, is required to detect the lensing contribution. Indeed, for a MAP type mission, the results in Table 2 show that gravitational lensing is difficult to detect in either temperature or polarisation spectra. However, for Planck the lensing effects might be significant in both power spectra and, despite the lower amplitude, are usually more easily detected in polarisation than in the temperature signal. In a Planck-like (or cosmic variance limited) experiment, the lensing contribution is measurable also in the cross-correlation power spectrum, though less easily than in the polarisation spectrum.

3.3 The dependence of gravitational lensing contributions on cosmological parameters

The dependence of the gravitational lensing contribution on cosmological parameters can be quantified by computing the derivatives of the lensed power spectra with respect to the cosmological parameter of interest. However, this presents a difficult numerical problem, because the lensing contribution is small and hence the derivatives can be easily swamped by numerical errors. In particular, the direct finite differencing scheme used to compute linear power spectrum derivatives (Bond et al. 1997, Zaldarriaga et al. 1997; Eisenstein et al. 1998, see also Section 4.2), cannot be applied to the lensed case given the typical numerical errors of $\sim 1\%$ in

CMB Boltzmann codes. Instead we have applied two different semi-analytical approaches based on numerical derivatives of the matter power spectrum rather than those of \tilde{C}_ℓ .

The derivative with respect to a cosmological parameter s_i can be expressed as ($I = T, E, C$),

$$\frac{\partial \tilde{C}_\ell^I}{\partial s_i} = \frac{\partial C_\ell^I}{\partial s_i} + \sum_{\ell'} \left[\frac{\partial W_{\ell\ell'}^I}{\partial s_i} C_\ell^I + W_{\ell\ell'}^I \frac{\partial C_\ell^I}{\partial s_i} \right] \quad (15)$$

where computing derivatives of the window functions W^I involves computations of the derivatives of the photon path dispersions $\sigma(\theta)$ and $\sigma_2(\theta)$.

In our first approach, derivatives of $\sigma^2(\theta)$, $\sigma_2^2(\theta)$ and C_ℓ are computed numerically by finite differencing. In the second method, only the derivative of C_ℓ is computed by finite differencing, and the derivatives of both $\sigma^2(\theta)$ and $\sigma_2^2(\theta)$ are calculated using numerically precomputed derivatives of the gravitational potential power spectrum $P_\phi(k, \eta)$. For example, derivatives of $\sigma^2(\theta)$ are obtained through the formula,

$$\begin{aligned} \frac{\partial \sigma^2(\theta)}{\partial s_i} &= 16\pi^2 \int_0^\infty dk k^3 \int_{a_{LS}}^{a_0} da \times \\ &\times \left\{ \frac{\partial P_\phi(k, a)}{\partial s_i} W^2 [1 - J_0(k\theta \sin_K \chi)] \frac{\partial \chi}{\partial a} \right. \\ &\left. + P_\phi(k, a) \frac{\partial}{\partial s_i} \left[W^2 [1 - J_0(k\theta \sin_K \chi)] \frac{\partial \chi}{\partial a} \right] \right\}, \end{aligned} \quad (16)$$

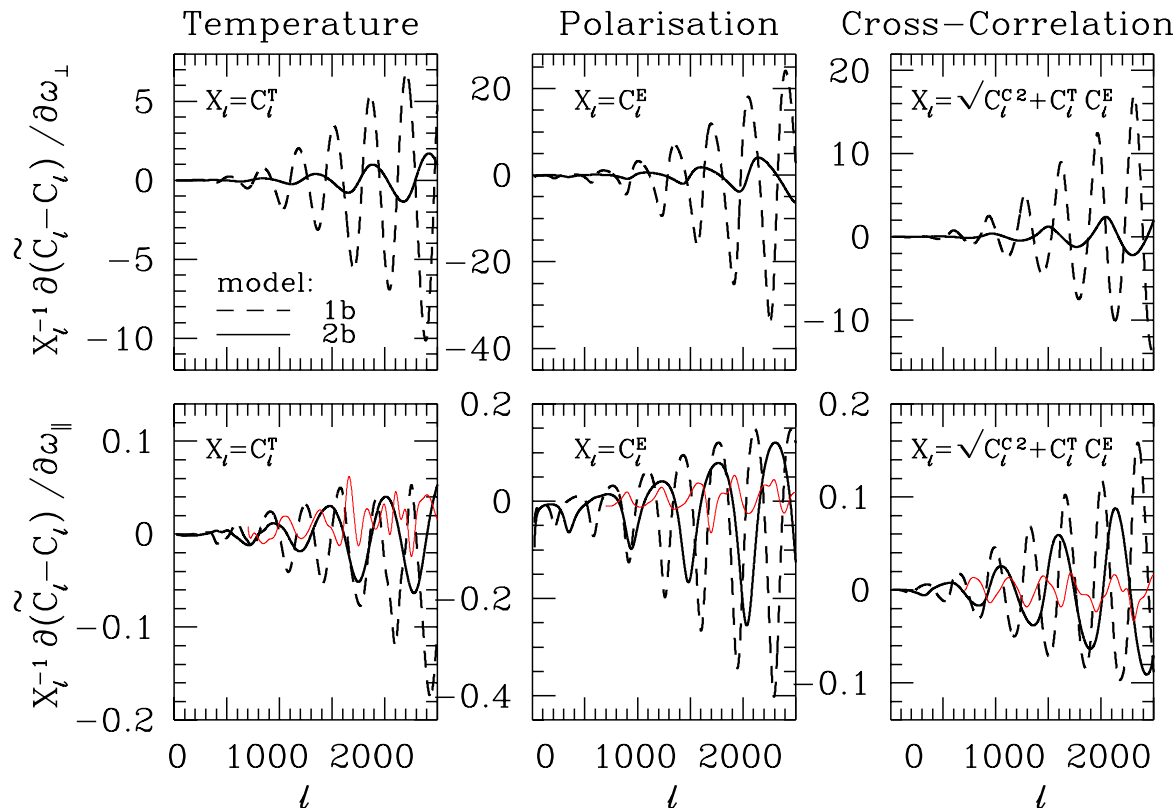


Figure 5. The derivatives of the gravitational lensing contribution to temperature (left panels), polarisation (middle panels) and cross-correlation (right panels) with respect to ω_{\perp} (upper row) and ω_{\parallel} (lower row) for models 1b and 2b. Dashed oscillatory lines show the derivatives for the spatially flat model (1b) and solid thick lines show the derivatives for the open model (2b). The thin solid lines in the lower panels show the linear power spectrum derivatives with respect to ω_{\parallel} , as plotted in Figure 4.

derived from equation (9). An analogous expression can be written for $\sigma_2^2(\theta)$. To compute the derivative of P_{ϕ} at any given value of the scale factor a , we assumed that P_{ϕ} grows according to linear theory, $P_{\phi}(k, a) = D^2(a, a_{LS})P_{\phi}(k, a_{LS})$, where $D(a, a_{LS})$ is the linear growth factor and depends only the scale factor and cosmological parameters. The growth factor has been computed directly by numerical integration of the set of linearized equations of motion (assuming Newtonian dynamics and a pressureless fluid). The derivatives of the growth factor have also been computed by integrating a set of derivatives of the equations of motion with respect to cosmological parameters.

For most target models that we have investigated, we find good agreement between the derivatives computed from the two methods described above. The second method is the more accurate, especially for cases where the parameter dependences of the lensed spectrum are weak, e.g. the derivative of \tilde{C}_l with respect to the residual optical depth for Thomson scattering. However, for most of the cosmological parameters, and in particular the derivatives with respect to curvature ω_K and ω_{Λ} , both methods fared equally well and we have chosen to use the first one since it is more computationally efficient.

The derivatives of the lensing corrections with respect to the parameters ω_K , ω_{Λ} and ω_{\parallel} are shown in Figure 5 for models 1b and 2b. These figures can be compared directly to

Figure 4 showing derivatives of the linear (unlensed) power spectra for these models.

Figure 5 shows that the gravitational lensing derivatives are small. This is because the matter power spectrum, on which the lensing correction depends via equations (5-10), is insensitive to many of the cosmological parameters. Furthermore, the main contribution to lensing comes from matter at relatively high redshifts, when the growth rates of perturbations are still largely insensitive to the cosmological model. Nevertheless, as we will show in the next Section, these weak dependences on cosmological parameters are potentially detectable and could break the geometrical degeneracy of linear CMB power spectra.

4 CMB CONSTRAINTS ON CURVATURE AND THE COSMOLOGICAL CONSTANT

4.1 The Fisher matrix formalism

For a vector \bar{x} of N Gaussian variables depending upon s_i ($i = 1, \dots, n$) parameters, an $n \times n$ Fisher matrix is defined as follows (e.g. Kendall & Stuart 1967, Tegmark, Taylor & Heavens 1997)

$$F_{ij} = \frac{\partial \bar{x}^T}{\partial s_i} \hat{M}^{-1} \frac{\partial \bar{x}}{\partial s_j}, \quad (17)$$

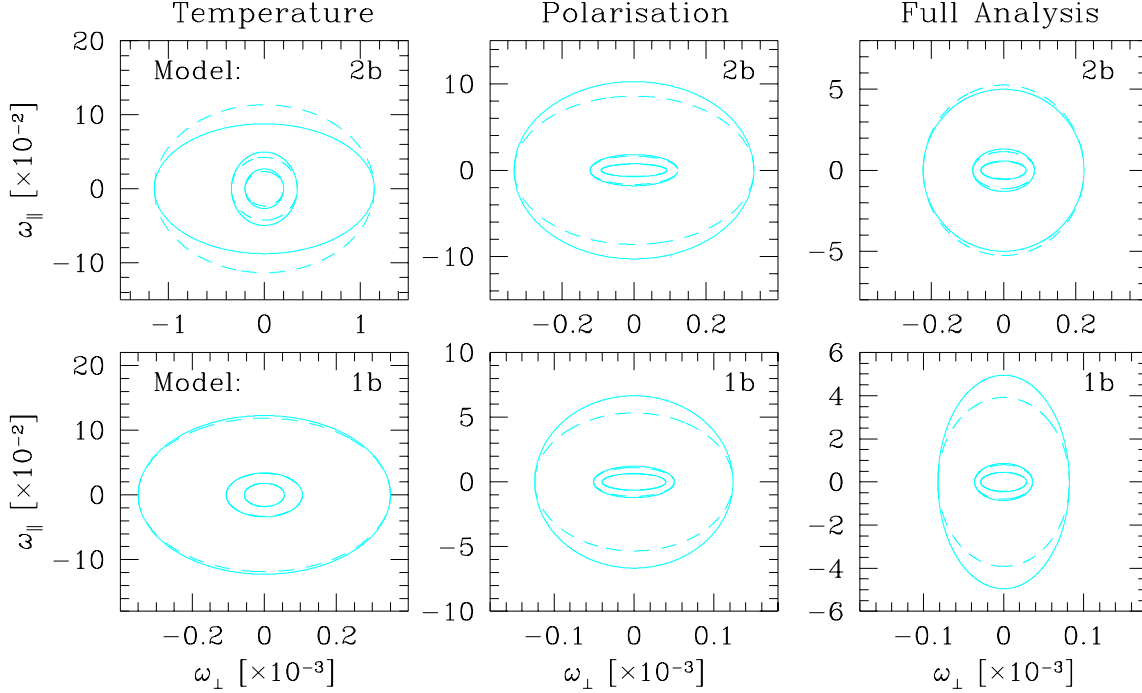


Figure 6. The 2σ constraints on the parameters ω_{\perp} and ω_{\parallel} (see eqn. (4) for a definition) derived from the Fisher matrix analysis described in the text. The results shown are for models 1b (bottom row) and 2b (upper row) and for three idealized cosmic variance limited experiments with $\ell_{\max} = 1000$ (giving the weakest constraints) 2000 and 2750 (giving the strongest constraints). The solid contours are derived from our numerical computations of the C_{ℓ} derivatives. The dashed lines assume vanishing linear C_{ℓ} derivatives along the degeneracy directions for $\ell \gtrsim 200$ (i.e. imposing the condition that the geometrical degeneracy is exact at high multipoles). The differences between the solid and dashed contours provide an estimate of the numerical errors in the computations of the Fisher matrix.

where \hat{M} denotes the correlation matrix of \bar{x} . For independent measurements of the temperature or polarisation power spectra, \bar{x} is a vector of the respective power spectrum coefficients and \hat{M} is diagonal with dispersions given by equation (14). The Fisher matrix in this case reads,

$$F_{ij}^{T,E} = \sum_{\ell=2}^{\ell_{\max}} \frac{\partial C_{\ell}^{T,E}}{\partial s_i} \Delta C_{\ell}^{T,E-2} \frac{\partial C_{\ell}^{T,E}}{\partial s_j}. \quad (18)$$

For a simultaneous analysis of all three power spectra we choose Transpose(\bar{x}) = $[C_2^T, C_2^E, C_2^C, \dots, C_{\ell}^T, C_{\ell}^E, C_{\ell}^C \dots]$, ensuring a block diagonal form of the \hat{M} matrix with 3×3 diagonal submatrices ($\equiv \hat{M}_{\ell}$) describing correlations of the $[C_{\ell}^T, C_{\ell}^E, C_{\ell}^C]$ vector. The appropriate Fisher matrix can be written as (Zaldarriaga et al. 1997, Kamionkowski, Kosowsky & Stebbins 1997),

$$F_{ij}^{T+E} = \sum_{\ell=2}^{\ell_{\max}} \sum_{I,J=\{T,E,C\}} \frac{\partial C_{\ell}^I}{\partial s_i} [M_{\ell}^{-1}]_{IJ} \frac{\partial C_{\ell}^J}{\partial s_j}, \quad (19)$$

where \hat{M}_{ℓ} is given by,

$$\begin{aligned} \hat{M}_{\ell}^{TT} &= \frac{2f_{sky}^{-1}}{2\ell+1} (C_{\ell}^T + w_T^{-1}b_{\ell}^{-2})^2 \\ \hat{M}_{\ell}^{TE} &= \frac{2f_{sky}^{-1}}{2\ell+1} C_{\ell}^T C_{\ell}^E \\ \hat{M}_{\ell}^{TC} &= \frac{2f_{sky}^{-1}}{2\ell+1} C_{\ell}^T (C_{\ell}^T + w_T^{-1}b_{\ell}^{-2}) \end{aligned} \quad (20)$$

$$\begin{aligned} \hat{M}_{\ell}^{EE} &= \frac{2f_{sky}^{-1}}{2\ell+1} (C_{\ell}^E + w_E^{-1}b_{\ell}^{-2})^2 \\ \hat{M}_{\ell}^{EC} &= \frac{2f_{sky}^{-1}}{2\ell+1} C_{\ell}^E (C_{\ell}^E + w_E^{-1}b_{\ell}^{-2}) \\ \hat{M}_{\ell}^{CC} &= \frac{f_{sky}^{-1}}{2\ell+1} [C_{\ell}^{C^2} + (C_{\ell}^T + w_T^{-1}b_{\ell}^{-2}) (C_{\ell}^E + w_E^{-1}b_{\ell}^{-2})] \end{aligned}$$

Finally, the inverse of the Fisher matrix F_{ij} is interpreted as the covariance matrix of the small parameter deviations ($\equiv \delta s_i$) from their target values. In particular, the i^{th} diagonal element of its inverse provides a lower bound on the standard error of the corresponding s_i parameter.

4.2 Numerical computations

The linear power spectra were computed using the CMBFAST code of Seljak & Zaldarriaga (1996), and their derivatives with respect to cosmological parameters were obtained by a direct finite differencing scheme. To improve the numerical accuracy, we used much finer grids in wavenumber and multipole and shorter integration timesteps than the default CMBFAST values. The importance of accurate derivatives of the CMB power spectrum in the computation of the Fisher matrix has been discussed recently by Bond et al. (1997), Efstathiou & Bond (1998) and Eisenstein et al. (1998). In particular, numerical errors in the derivatives required for the Fisher matrix can easily lead to a spurious breaking of the geometrical degeneracy. An accurate de-

Table 3. 68.5% (1σ) uncertainties (multiplied by a factor of 100) for ω_K and ω_Λ determinations (with all other parameters fixed) obtained through the Fisher matrix analysis of the CMB power spectrum with gravitational effects included. The results of the analysis based on either temperature or polarisation information are denoted by T and E , respectively, while the results of the full analysis are denoted as TEC . The table lists results for the $h = 0.5$ models only.

Experiment	$\delta\omega_K [\times 10^{-2}]$,			$\delta\omega_\Lambda [\times 10^{-2}]$		
	T	E	TEC	T	E	TEC
• standard CDM model						
	$(\omega_m = 0.25, \omega_b = 0.0125, \omega_K = 0, \omega_\Lambda = 0, \sigma_8(t_0) = 0.52)$					
$l_{max} = 1000$	2.1	0.8	0.4	14.0	5.5	2.8
$l_{max} = 2000$	0.5	0.15	0.1	3.25	1.1	0.7
$l_{max} = 2750$	0.15	0.075	0.045	0.85	0.5	0.3
Planck	1.1	2.6	0.8	7.4	17.1	5.5
• model 1a:						
	$(\omega_m = 0.1, \omega_b = 0.0125, \omega_K = 0, \omega_\Lambda = 0.15, \sigma_8(t_0) = 0.8)$					
$l_{max} = 1000$	0.45	0.2	0.15	5.3	2.3	1.5
$l_{max} = 2000$	0.15	0.045	0.03	1.5	0.5	0.35
$l_{max} = 2750$	0.075	0.025	0.02	0.8	0.3	0.2
Planck	0.2	0.2	0.1	2.1	2.4	1.2
• model 2a:						
	$(\omega_m = 0.1, \omega_b = 0.0125, \omega_K = 0.15, \omega_\Lambda = 0, \sigma_8(t_0) = 0.8)$					
$l_{max} = 1000$	1.2	1.1	0.6	3.5	3.5	1.7
$l_{max} = 2000$	0.55	0.2	0.15	1.6	0.65	0.4
$l_{max} = 2750$	0.3	0.09	0.065	0.9	0.27	0.2
Planck	0.5	0.65	0.3	1.5	2.0	0.9

termination of the Fisher matrix is especially important in the analysis described here, because we want to investigate whether a real physical effect, rather than numerical errors, can break the geometrical degeneracy.

The accuracy of CMBFAST was tested by measuring derivatives of linear power spectra along the geometrical degeneracy line (i.e. with respect to ω_{\parallel}) as shown by the thin solid lines in the lower panels of Figure 5. The residuals are significantly smaller than the derivatives of the lensing corrections. As we will demonstrate in the next section, these errors do not affect the Fisher matrix coefficients significantly when lensing is included. Also the results of Fisher matrix analysis do not depend on the choice of the initial parametrization demonstrating that our linear power spectrum derivatives are not significantly affected by numerical errors.

4.3 Fisher matrix analysis of CMB spectra

To analyse the degree to which the degeneracy can be broken by the lensing contribution we compute the C_ℓ derivatives and hence the Fisher matrix of the power spectra including the gravitational lensing contribution. We assume that the lensed CMB anisotropies are Gaussian. On the angular scales probed by MAP and Planck, the non-Gaussianities introduced by gravitational lensing should be negligible (see Bernardeau 1997). We first analyse the effects of gravitational lensing in the two-dimensional space defined by ω_K and ω_Λ , to show that lensing does break the geometrical degeneracy if all other parameters are known. We then analyse

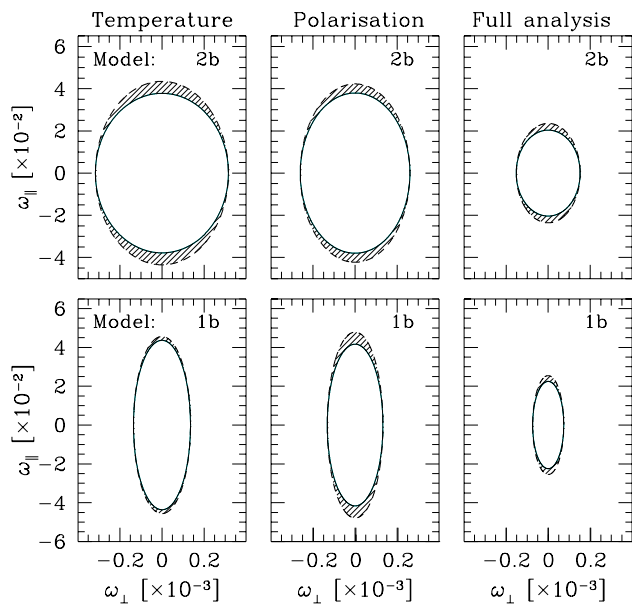


Figure 7. 2σ contours in $(\omega_{\perp}, \omega_{\parallel})$ plane for a Planck-type experiment. The width of the shaded regions shows the effect of the numerical inaccuracies on our final results.

a more realistic example varying six cosmological parameters.

4.3.1 Variations of ω_K and ω_Λ

The Fisher matrix results restricting to the two parameters ω_K and ω_Λ are presented in Table 3 and in Figures 6 & 7. In these Figures we plot 2σ error ellipses in the plane $(\omega_{\parallel}, \omega_{\perp})$ defined as in equation (4), i.e. in the directions parallel and perpendicular to the geometrical degeneracy direction. In each case, the solid contours were derived by computing the numerical derivatives of the linear and lensing corrections with respect to both parameters (as shown in Figures 4 and 5). The dashed contours were computed by setting the derivative of the linear power spectra along the degeneracy direction to zero at multipoles $\ell \gtrsim 200$. The differences between the solid and dashed lines thus provide an indication of the effects of numerical errors on the Fisher matrix analysis. For both temperature and polarisation anisotropies, gravitational lensing *breaks the geometrical degeneracy* and leads to useful constraints on ω_{\parallel} . For example, for a Planck-type experiment and the two models shown in Figure 7 [models 1b and 2b, normalised to have $\sigma_8(t_0) = 0.95$], the inclusion of gravitational lensing leads to a 2σ error of $\omega_{\parallel} \approx 0.05$ and an even a stricter constraint on ω_Λ . The constraints are less strong for models with lower amplitude at the high redshifts (as a result of the normalisation of the present day matter fluctuations or/and their higher growth rates) and hence smaller CMB lensing contributions. In the case of the standard CDM model listed in Table 3, the 1σ constraints on ω_Λ and ω_K when polarisation and temperature information are combined are $\delta\omega_\Lambda \approx 0.05$ and $\delta\omega_K \approx 0.008$. These constraints are considerably worse than those for models 1a and 2a listed in Table 3, which have a higher amplitude of mass fluctuations. Nevertheless,

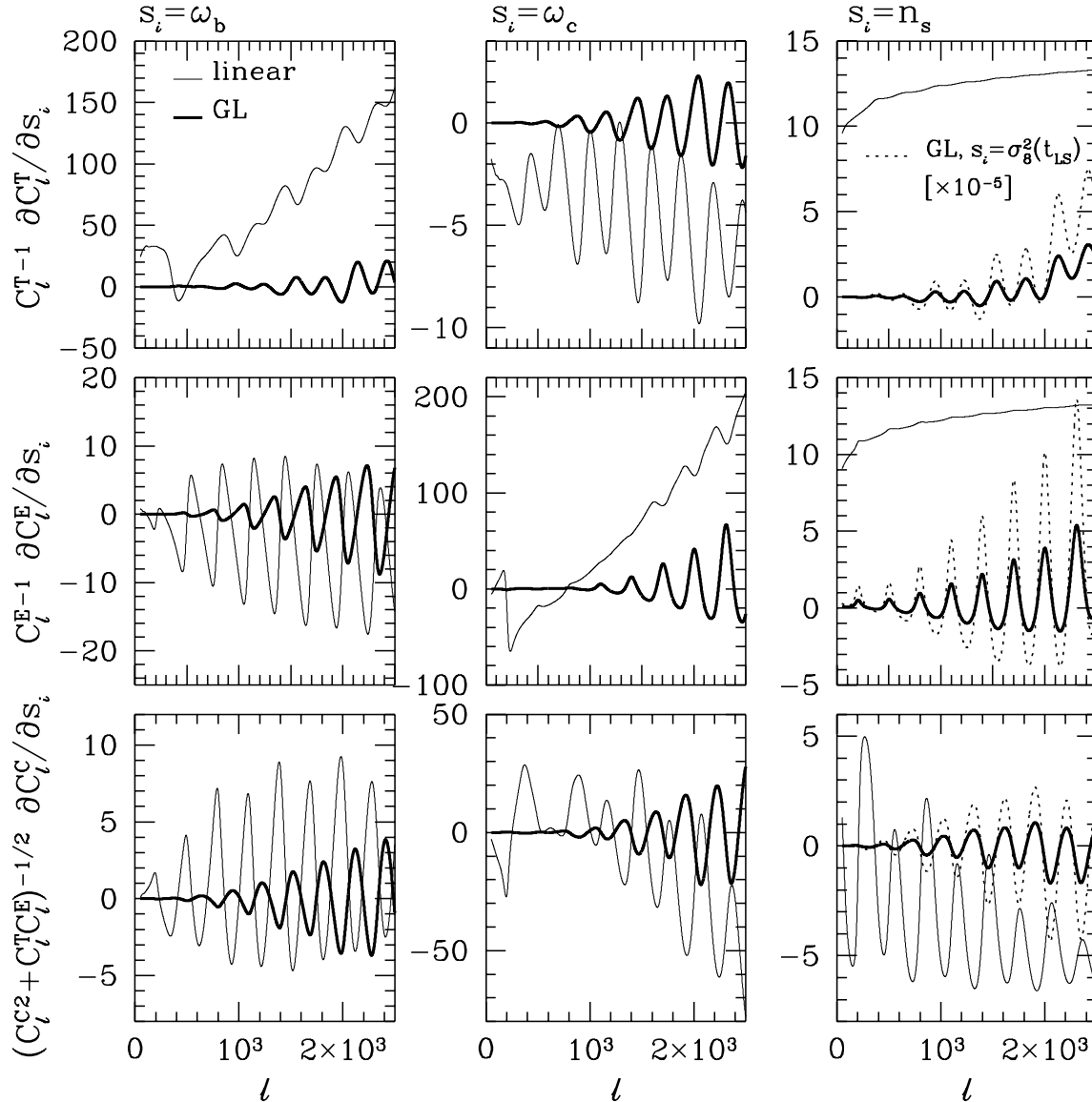


Figure 8. Examples of linear power spectrum and gravitational lensing contribution derivatives for the SCDM model (see Table 1) with respect to three cosmological parameters. The solid thin line in each panel shows the linear power spectrum derivative, while thick lines show the derivative of the lensing contribution (with respect to the parameter given at the top of the picture). In addition the gravitational lensing contribution derivative with respect to an amplitude [defined as $\sigma_8^2(t_{LS})$ and expressed in units 10^{-5}] is shown as dotted lines in the rightmost panels.

even for the standard CDM model, the constraints on ω_Λ and ω_K are still interesting.

4.3.2 Variations of 6 cosmological parameters

The results of the previous section show that a Planck-type experiment is sensitive to gravitational lensing of the CMB and that gravitational lensing can break the geometrical degeneracy. There is, however, a possibility that the lensing contributions to the CMB anisotropies can be mimicked by variations in other cosmological parameters thereby defining a new degeneracy direction. It is unlikely that such a degeneracy would be perfect, but it is possible that the the total

power spectra including lensing corrections are partially degenerate with respect to variations of other parameters, limiting their usefulness as a diagnostic of the geometry of the Universe. To examine this possibility we have therefore computed the Fisher matrix for a more realistic six parameter space defined by the following cosmological parameters: ω_K , ω_Λ , ω_b , ω_c , the scalar spectral index n_s and the amplitude $\sigma_8(t_{LS})$ of the mass fluctuations at the time of recombination. We have explicitly ignored a tensor component since any tensor component would have a negligible amplitude at the high multipoles at which gravitational lensing of the CMB is significant.

The results of the Fisher matrix analysis for a Planck-

Table 4. Forecasted accuracy (1σ) of the determination of the selected cosmological parameters as obtained through Fisher matrix analysis of the six dimensional parameters space with additional external constraints imposed within a 2DIM (ω_K, ω_Λ) plane and a gravitational lensing effect either excluded (i.e. linear radiation power spectrum only) or included as indicated. Presented results are for a Planck-like experiment measuring the C^T , C^E and C^C power spectra (see text for details)

	GL	$\delta\omega_b$	$\delta\omega_c$	$\delta\omega_K$	$\delta\omega_\Lambda$	δn_s	$\frac{\delta\sigma_8(t_{LS})}{\sigma_8(t_{LS})}$
	contr.	$[\times 10^{-5}]$	$[\times 10^{-3}]$	$[\times 10^{-2}]$	$[\times 10^{-2}]$	$[\times 10^{-3}]$	$[\times 10^{-2}]$
• SCDM:		$\omega_b = 0.0125$	$\omega_c = 0.2375$	$\omega_K = 0$	$\omega_\Lambda = 0$	$n_s = 1$	$\sigma_8(t_0) = 0.52$
full 6D case:	yes	6.2	2.6	1.0	6.3	2.9	1.9
2D case:	yes	–	–	0.8	5.5	–	–
ω_\parallel fixed:	yes	6.1	2.3	0.1	0.014	2.9	1.8
	no	5.9	2.4	0.1	0.015	3.1	2.0
ω_Λ fixed:	yes	5.6	1.3	0.06	–	2.8	1.7
	no	5.3	1.3	0.06	–	3.0	1.8
ω_K fixed:	yes	6.1	2.5	–	0.7	2.9	1.8
	no	6.0	2.7	–	0.7	3.1	2.0
• model 1a:		$\omega_b = 0.0125$	$\omega_c = 0.0875$	$\omega_K = 0$	$\omega_\Lambda = 0.15$	$n_s = 1$	$\sigma_8(t_0) = 0.8$
full 6D case:	yes	4.2	0.4	0.3	3.4	2.1	1.3
2D case:	yes	–	–	0.1	1.2	–	–
ω_\parallel fixed:	yes	4.2	0.24	0.01	0.001	1.8	1.0
	no	4.1	0.17	0.009	0.0008	2.3	1.3
ω_Λ fixed:	yes	4.2	0.2	0.01	–	1.9	1.0
	no	4.1	0.15	0.008	–	2.3	1.3
ω_K fixed:	yes	4.5	0.5	–	0.3	1.5	0.8
	no	4.2	0.7	–	0.4	2.6	1.8
• model 2a:		$\omega_b = 0.0125$	$\omega_c = 0.0875$	$\omega_K = 0.15$	$\omega_\Lambda = 0$	$n_s = 1$	$\sigma_8(t_0) = 0.8$
full 6D case:	yes	4.0	0.4	0.7	1.9	1.5	0.7
2D case:	yes	–	–	0.3	0.9	–	–
ω_\parallel fixed:	yes	3.9	0.24	0.06	0.02	1.4	0.6
	no	3.6	0.23	0.06	0.02	1.6	0.8
ω_Λ fixed:	yes	3.8	0.2	0.05	–	1.4	0.6
	no	3.6	0.2	0.05	–	1.6	0.7
ω_K fixed:	yes	3.9	0.2	–	0.2	1.4	0.6
	no	3.6	0.2	–	0.2	1.6	0.8

type experiment are listed in Table 4. The errors on ω_Λ and ω_K for the standard CDM model in the six parameter example are usually larger than those of the idealized two parameter example described in the previous subsection. For example for models 1a (Λ -dominated, spatially flat universe) and 2a ($\Lambda = 0$, open universe), the errors on ω_Λ and ω_K in the six-dimensional case are about 2 – 3 times those derived for the two-dimensional case. However, no new near-degeneracy is found suggesting that it is feasible to separate the geometrical dependence of the lensing contributions of the CMB power spectra from the changes caused by varying other cosmological parameters.

5 SUMMARY

Observations of the CMB anisotropies promise a dramatic improvement in our knowledge of the formation of cosmic structure and of the values of fundamental cosmological parameters that define our Universe. According to linear perturbation theory, however, there exists a near exact geometrical degeneracy that makes it nearly impossible to disentangle the values of Ω_K and Ω_Λ from observations of the CMB anisotropies alone. In reality, the CMB temperature

and polarisation anisotropies will be modified by gravitational lensing caused by the irregular distribution of matter between us and the last scattering surface. The effects of gravitational lensing, although small, might be detectable by the Planck satellite for reasonable values of the amplitude of the present day mass fluctuations (i.e. values that reproduce the present day abundance of rich clusters of galaxies).

In this paper, we have computed the effects of gravitational lensing on both the temperature and polarisation pattern and demonstrated that lensing can break the geometrical degeneracy inherent in the linear CMB power spectra. We have performed a Fisher matrix analysis to show how gravitational lensing affects estimates of cosmological parameters. The Fisher matrix requires derivatives of the CMB power spectra with respect to the cosmological parameters. Since numerical errors in these derivatives can artificially break real parameter degeneracies, we have made a detailed analysis of numerical errors in our computations and shown that they are small.

The results of our Fisher matrix analysis are summarized in Tables 3 & 4 for an idealized two dimensional space of ω_Λ and ω_K and for a more realistic space of six cosmological parameters. These show that gravitational lensing is detectable by a Planck-type experiment and must be taken

into account when estimating the values of cosmological parameters. The effects of gravitational lensing are detectable in both the temperature and polarisation anisotropies. For some experimental parameters, the effects of lensing are more easily detectable in the polarisation signal (because of the sharpness of the peaks and minima in the polarisation power spectrum) than in the temperature power spectrum, even though the anisotropies are polarised at only the few percent level. Gravitational lensing of the CMB anisotropies breaks the geometrical degeneracy and so it should be possible to set limits on the values of ω_Λ and ω_K from observations of the CMB anisotropies alone. For example, from the 6 parameter analysis in Table 4 for model 1a (a spatially flat Λ -dominated universe) it should be possible to set 1σ limits of $\delta\omega_\Lambda \approx 0.03$ and $\delta\omega_K \approx 0.003$ using temperature and polarisation measurements and limits of $\delta\omega_\Lambda \approx 0.04$ and $\delta\omega_K \approx 0.004$ from observations of temperature anisotropies alone. This shows that for certain target models a Planck-type experiment is capable of setting tight limits on the geometry of the Universe. Furthermore, the possibility of detecting gravitational lensing adds to the scientific case for measuring CMB polarisation at high sensitivity and angular resolution.

The lensing constraints on ω_Λ and ω_K are sensitive to the normalisation of the present day mass fluctuations and the growth rate of the matter fluctuations hence we find less stringent limits for a standard CDM model normalised to $\sigma_8(t_0) = 0.52$ (Tables 3 and 4). Nevertheless, even in this case, a Planck-like experiment can set 1σ errors of $\omega_\Lambda \approx 0.06$ and $\omega_K = 0.01$.

The geometrical degeneracy can be broken by applying constraints derived from more conventional astronomical techniques. For example, accurate measurements of the Hubble constant, age of the Universe, the luminosity distances of Type 1a supernovae, measurements of large-scale galaxy clustering can be used, with various assumptions, to break the geometrical degeneracy (see Efstathiou & Bond 1998). However, as described in this paper, gravitational lensing breaks the geometrical degeneracy and so one can disentangle the values of Ω_K and Ω_Λ from accurate observations of the CMB anisotropies. Comparison of results of CMB-based experiments with those obtained with more conventional techniques can provide consistency checks and tests of possible systematic errors.

Acknowledgements GPE would like to thank PPARC for the award of a Senior Research Fellowship. RS is supported by UK PPARC grant and acknowledges help of Polish Scientific Committee (KBN) grant No. 2 P03D 008 13.X2. We thank the referee Matias Zaldarriaga for many useful comments and for encouraging us to include the temperature-polarisation power spectrum in the Fisher matrix analysis of Section 4.

REFERENCES

- Barsanelli M. et al., 1996, COBRAS/SAMBA, The Phase A Study for an ESA M3 Mission, ESA Report, D/SCI (96/3)
- Bennett C.L. et al., 1996, ApJ, 464, 1
- Bennett C.L. et al., 1997, Bull. American. Astron. Soc., 191, #87.01
- Bernardeau F., 1997, A&A, 324, 15
- Blanchard A., Schneider J., 1987, A&A, 184, 1
- Bond J. R., 1996, in Schaeffer R., ed. Les Houches Session LX, Cosmology and Large-Scale Structure, Elsevier Science Press, Dordrecht
- Bond J.R., Efstathiou G., 1984, ApJ, 285, L45
- Bond J.R., Efstathiou G., Tegmark M., 1997, MNRAS, 291, L31
- Bond, J.R., Jaffe A., 1997, in Microwave Background Anisotropies, ed F. Bouchet et al. (Editiones Frontieres, Singapore). astro-ph/9610091.
- Bunn E.F., Scott D., White M., 1995, ApJ, 441, 53
- Caldwell R., Dave R., Steinhardt P., 1998, astro-ph/9708069
- Cole S., Efstathiou G., 1989, MNRAS, 239, 195
- Doroshkevich A.G., Zel'dovich Ya.B., Sunyaev R.A., 1978, Sov. Astron., 22, 523
- Efstathiou G., Bond J.R., 1998, submitted to MNRAS, astro-ph/9807103
- Eke V.R., Cole S., Frenk C.S., 1996, MNRAS, 282, 263
- Eisenstein, D.J., Hu W., Tegmark, M., 1998, submitted to ApJ, astro-ph/9807130
- Górski K.M., Ratra B., Stompor R., Sugiyama N., Banday A.J., 1998, ApJS, 114, 1
- Hancock S., Gutierrez C.M., Davies R.D., Lasenby A.N., Rocha G., Rebolo R., Watson R.A., Tegmark M., 1997, MNRAS, 289, 505
- Harrison E.R., 1967, Rev. Mod. Phys., 39, 862
- Hu W., Sugiyama N., 1995, ApJ, 444, 489
- Hu W., White M., ApJ, 1997, 479, 568
- Huey G., Wang L., Dave R., Caldwell R.R., Steinhardt P.J., 1998, submitted to Phys. Rev. D, astro-ph/9804285
- Jungman G., Kamionkowski M., Kosowsky A., Spergel D.N. 1996, Phys. Rev. D48, 3502
- Kamionkowski M., Kosowski A., Stebbins A., 1997, Phys. Rev. D55, 7368
- Kendall M.G., Stuart A., 1967, "The Advanced Theory of Statistics", vol. 2, 2nd Edition, Griffin & Company
- Lineweaver C.H., Barbosa D., Blanchard A., Bartlett J.G., 1997, A&A, 322, 365
- Martínez-González E., Sanz J.L., Cayón L., 1997, ApJ, 484, 1
- Metcalfe R.B., Silk J.I., 1998, ApJ, 492, 1
- Peacock J.A., Dodds S.J., 1996, MNRAS, 180, 19
- Peebles P.J.E., 1968, ApJ, 153, 1
- Peebles P.J.E., Yu J.T., 1970, ApJ, 162, 815
- Puget J.L., et al., 1998, "High-Frequency Instrument for the Planck Mission", proposal submitted to ESA Announcement of Opportunity, February 1998.
- Ratra B., Peebles P.J.E., 1988, Phys. Rev. D37, 3406
- Sasaki M., 1989, MNRAS, 240, 415
- Seljak U., 1996, ApJ, 463, 1
- Seljak U., Zaldarriaga M., 1996, ApJ, 469, 437
- Stompor R., Górski K.M., Banday A.J., 1995, MNRAS, 277, 1225
- Tegmark M., Taylor A.N., Heavens A.F., 1997, ApJ, 480, 22
- Tegmark M., Eisenstein D.J., Hu W., 1998, To appear in Fundamental Parameters in Cosmology, Rencontres de Moriond 1997, in press, astro-ph/9804168
- Turner M.S., White M., 1997, Phys. Rev. D56, R4439
- Viana P.T.P., Liddle A.R., 1996, MNRAS, 281, 323
- Vittorio N., Silk J.I., 1984, ApJ, 285, L39
- White M., 1998, submitted to ApJ, astro-ph/9802295
- Wilson M.L., Silk J.I., 1981, ApJ, 243, 14
- Zaldarriaga M., Spergel D.N., Seljak U., 1997, ApJ, 488, 1
- Zaldarriaga M., Seljak U., 1998, Phys. Rev. D58, 023003